Journal of the Korean Ceramic Society
Vol. 53, No. 3, pp. 301~305, 2016.

http://dx.doi.org/10.4191/kcers.2016.53.3.301

Proton Conduction in Nonstoichiometric ∑3 $BaZrO_3$ (210)[001] Tilt Grain Boundary Using Density Functional Theory

Ji-Su Kim* and Yeong-Cheol Kim*,,†**

**School of Energy Materials and Chemical Engineering, KoreaTech, Cheonan 31253, Korea*
***Materials Research Center, KoreaTech, Cheonan 31253, Korea*

(Received March 29, 2016; Revised April 28, 2016; Accepted May 2, 2016)

ABSTRACT

We investigate proton conduction in a nonstoichiometric ∑3 $BaZrO_3$ (210)[001] tilt grain boundary using density functional theory (DFT). We employ the space charge layer (*SCL*) and structural disorder (*SD*) models with the introduction of protons and oxygen vacancies into the system. The segregation energies of proton and oxygen vacancy are determined as -0.70 and -0.54 eV, respectively. Based on this data, we obtain a Schottky barrier height of 0.52 V and defect concentrations at 600K, in agreement with the reported experimental values. We calculate the energy barrier for proton migration across the grain boundary core as 0.61 eV, from which we derive proton mobility. We also obtain the proton conductivity from the knowledge of proton concentration and mobility. We find that the calculated conductivity of the nonstoichiometric grain boundary is similar to those of the stoichiometric ones in the literature.

Key words : Proton conduction, Nonstoichiometric grain boundary, Density functional theory, Space charge layer

1. Introduction

Iwahara *et al.* first reported the proton conduction in the perovskite structures such as $SrZrO_3$ and $SrCeO_3$ in 1980, and many following studies have been carried out on the phenomena taking place in the interior of oxides.[1-2] Among many proton-conductors, the acceptor-doped barium zirconate ($BaZrO_3$, BZO) has been intensively studied as an electrolyte of protonic ceramic fuel cell (PCFC) because of its high proton conductivity through the grain interior and sound chemical stability.[3-12] However, the low proton conductivity across the grain boundary compared to that of grain interior has been recognized as a critical issue.[3-13]

The low proton conductivity of BZO grain boundary has been often interpreted with the space charge layer (*SCL*) model, in which the positively charged protons accumulate in grain boundary.[3-13] Another model, the structural disorder (*SD*) model, has attributed the cause of low proton conductivity to the increased energy barrier for proton transport by the disordered grain boundary.[3] Recently, Yang *et al.* proposed an hybrid model of *SCL* and *SD* models, and investigated proton conductivity of a ∑3 BZO (111)[1$\bar{1}$0] grain boundary by using density functional theory (DFT).[13]

Studies on *SCL* formation focused mainly on the stoichiometric BZO grain boundary, and rarely on the nonstoichiometric ones.[9-13] Helgee *et al.*, for example, investigated *SCL* formation for three stoichiometric BZO cases using DFT; ∑3 (110)[1$\bar{1}$0], ∑3 (112)][1$\bar{1}$0], and ∑3 (210)[001] BZO grain boundaries.[9] They confirmed that Schottky barrier heights are in the same range of 0.6 V at 600K although the grain boundary structures are different.[9] Polfus *et al.* also investigated the *SCL* formation on a stoichiometric ∑3 BZO (111)[1$\bar{1}$0] grain boundary using DFT, and reported the height of 0.51 V at 573K.[10] These two studies indicate that Schottky barrier heights are not affected much by the orientation of the grain boundaries.

Only limited studies are available for the nonstoichiometric grain boundary structures such as $SrTiO_3$ and $BaTiO_3$.[14-15] Kim *et al.* studied $SrTiO_3$ structure by STEM (scanning transmission electron microscope), and found that the grain boundary is nonstoichiometric.[14] Choi *et al.* measured the Ba/Ti ratio of $BaTiO_3$ by HREM (high resolution electron microscope), and mentioned that the grain boundary compared to the bulk grain has more Ti atoms.[15] Recently, Kim *et al.* evaluated stability of the nonstoichiometric ∑3 BZO (210)[001] grain boundary in terms of oxygen partial pressure and oxygen chemical potential using DFT, and reported that the nonstoichiometric grain boundary is more stable compared to the stoichiometric one.[16]

Thus, proton conductivity evaluation at the operation temperature of PCFC with a stable nonstoichiometric BZO grain boundary is important. We design a grain boundary of nonstoichiometric ∑3 BZO (210)[001] for this study by following the *SCL* model, and calculate the Schottky barrier height and estimate the concentration of proton. We calculate the energy barrier of proton along the minimum trans-

†Corresponding author : Yeong-Cheol Kim
E-mail : yckim@kut.ac.kr
Tel : +82-41-560-1326 Fax : +82-41-560-1360

port path, and estimate the proton mobility based on it. We also calculate proton conductivity with proton concentration and its mobility at the grain boundary of the system, and compare it with other reported experimental and theoretical results.

2. Calculation Details

All calculations in this study were carried out within the framework of the DFT using the Vienna Ab-initio Simulation Package (VASP).[17-20] Electron wave function was described by the Blöchl's projector augmented wave (PAW) method formulated by Kresse and Joubert[21-22] with the exchange- correlation energy of Perdew-Burke-Ernzerhof (PBE) parameterization within the generalized gradient approximation (GGA).[23-24] We considered the strong correlation effect for Zr atom by using U_{eff} (U - J) of 3 eV proposed by Vladan *et al.* in their study on the formation energy correction for oxides.[25]

We used a cutoff energy of 500 eV, and generated a k-point grid of 8×8×8 by the *Monkhorst-Pack* method.[26] The orbital occupation by electron at the Fermi level was smeared by the Gaussian method with a smearing factor of 0.05 eV. Electronic and ionic minimizations were carried out until total energy convergence of less than 10^{-4} and 10^{-3} eV, respectively. The geometric structure was optimized until each atom's residual force falls below 0.02 eV/Å. We also analyzed the electronic structure of grain boundary using Bader charge calculation.[27] The energy barrier for proton transport was determined by using the climbing image nudged elastic band (CINEB) method.[28] All illustrations were drawn by using the Visualization for Electronic and Structural Analysis (VESTA) program.[29]

Figure 1(a) shows the perspective view of the optimized BZO unit cell with a lattice constant of 0.428 nm, in agreement with the experimental value of 0.415 nm.[30] Fig. 1(b) is the (210) surface of a 2 × 2 × 2 $BaZrO_3$ super cell formed with BaO and ZrO_2 planes. Note that Kim *et al.* formed stoicheometric and nonstoicheometric ∑3 $BaZrO_3$ (210)[001] grain boundaries using the same BaO and ZrO_2 planes, and computationally evaluated its stability in terms of temperature, pressure, and chemical potential.[16] Fig. 1(c) represents the nonstoicheometric ∑3 $BaZrO_3$ (210)[001] grain boundary, which is found to be the most stable.

We introduced the *SCL* model in order to calculate the electrostatic potential, and concentration (c_D, $D = H$ or V) of proton (H) and oxygen vacancy (V) formed in grain boundary.[6-11,31] Dopant concentration of 10% was assumed to be uniformly distributed in the grain boundary structure by following the Mott-Schottky approximation. The partial pressure of water and dielectric constant were set as 0.025 atm and 75, respectively.[3,13] The hydration enthalpy and entropy in grain interior were set at –0.79 eV and –0.89 meV/K, respectively.[3,13] Mobility of H (μ_H) was calculated by the following equation.

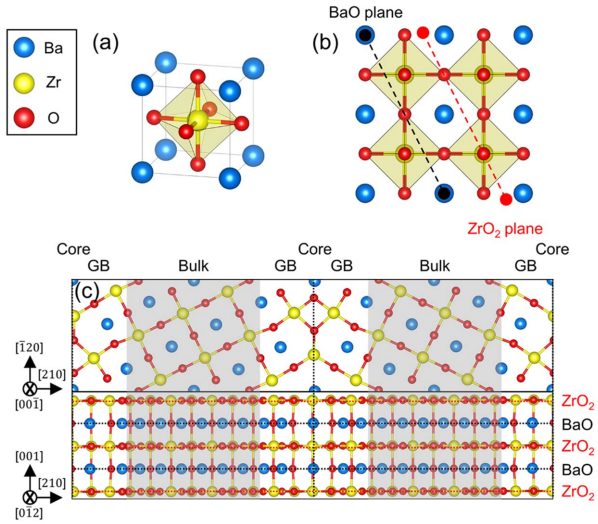

Fig. 1. (a) Perspective view of a $BaZrO_3$ unit cell, (b) planar view of a 2 × 2 × 2 $BaZrO_3$ super cell, (c) planar and top views of a nonstoichiometric ∑3 BZO (210)[001] tilt grain boundary. The black and red dashed lines in (b) indicate BaO and ZrO_2 planes, respectively.

$$\mu_H = \frac{D_0 q_H}{k_B T} exp\left(\frac{-E_m}{k_B T}\right) \quad (1)$$

Here, D_0 is the maximum diffusion coefficient, q_H is the charge of H, E_m is the transport energy barrier of H, k_B is the Boltzmann's constant, and T is temperature. Conductivity of H (σ_H) is calculated by the following equation using the concentration and mobility of H (c_H and μ_H).

$$\sigma_H = c_H \cdot q_H \cdot \mu_H$$

Readers may refer to the paper by Yang *et al.* for details of *SCL* model and σ_H.[13]

3. Results and Discussion

Figure 2 shows Bader (B_i, i = Ba, Zr, O) charges of (a) Ba, (b) Zr, and (c) O atom in the nonstoichiometric ∑3 BZO (210)[001] grain boundary along the distance from the grain boundary core (z = 0). The black square, black circle, black triangle, and empty triangle indicate the B_{Ba}, B_{Zr}, B_O in the ZrO_2 layer, and B_O in the BaO layer, respectively. The vertical dashed line represents the grain boundary core (z = 0), and white and grey regions are grain boundary and grain interior, respectively. In the grain boundary core, B_{Ba} became more positive, B_O less negative, and B_{Zr} less positive compared with their bulk values.

Since O atoms coordinate with two and three Zr atoms in grain interior and grain boundary, respectively, the O atoms in grain boundary are positively charged compared to the other case. Charges of B_{Ba} and B_{Zr} in grain interior converged to 1.55 and 2.60 e, respectively. B_O in the BaO and ZrO_2 layers converged to 1.35 and 1.40 e, respectively. This

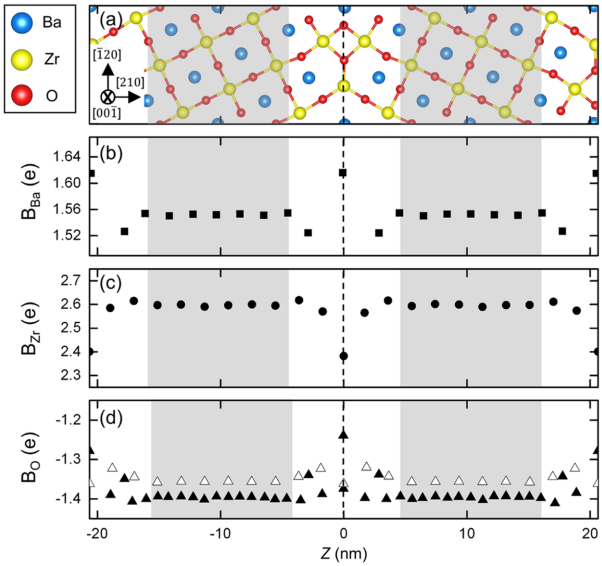

Fig. 2. A planar view of (a) the nonstoichiometric ∑3 BZO (210)[001] tilt grain boundary and Bader charges (B_i i= Ba, Zr, and O) of (b) Ba, (c) Zr, (d) O atoms as a function of Z. The black square, black circle, black triangle, and empty triangle correspond to the B_{Ba}, B_{Zr}, B_O at ZrO_2 layer, and B_O at BaO layer respectively. The vertical dashed line indicates grain boundary core (Z = 0).

may attribute to the difference in atomic arrangement in the BaO and ZrO_2 layers. We also confirmed that B_{Ba} and B_{Zr} are symmetric along the base line of Z = 0, but B_O is slightly asymmetric.

Figure 3 shows the ∑3 BZO (210)[001] grain boundary, and changes of H and V formation energy (E_D, $D = H$ or V) along the distance from Z = 0. We calculated E_D by the following equation.

$$E_D = E_D^{GB} - E_D^{B}$$

Here, E_D^{GB} and E_D^{B} are energies when H or V is in the grain boundary or in the grain interior , respectively. We determined E_D^{B} as the reference defect energy when the charged defect is located far from the grain boundary core. In the figure, the black square and grey circle are E_H and E_V, respectively, and the vertical dashed line indicates the grain boundary core (Z = 0). Note the presence of O sites with higher E_H and E_V in the core compared to the grain interior.

O atoms coordinated with three Zr atoms have positive charges compared to O atoms in the grain interior, which leads to the formation of H or V and likely makes the grain boundary rather unstable. E_H in the grain boundary core is in the range of -1.16 ~ 0.58 eV, which is indicative of a stable segregation of H to the grain boundary. Note also that E_H in the grain boundary region is asymmetric, which may be due to the changed B_O from structural variation. V also could stably segregate to the grain boundary region, and its

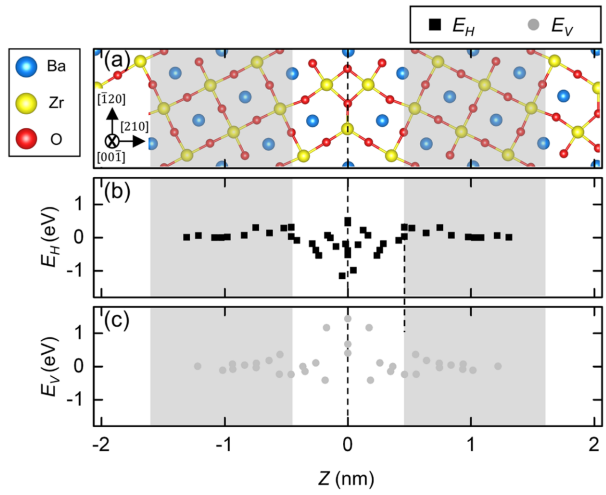

Fig. 3. A planar view of (a) the nonstoichiometric ∑3 BZO (210)[001] tilt grain boundary, and defect formation energy (E) as a function of the (b) proton and (c) oxygen vacancy position from the grain boundary core (z).

E_V is in the range of –0.6 ~ 0.6 eV.

Yang *et al.* considered the multi-H (multi-proton) effect to calculate the segregation energy ($E_{H,seg}$) more precisely. They averaged E_H for the excessively-segregated H adjacent to the grain boundary core.[13] Under the hydration condition, however, there is no need to consider the multi-V effect, since its concentration is very low in the core.[9-13,16] We further clarified that H can segregate easier to the grain boundary compared to V, since $E_{H,seg}$ (–0.70 eV) is lower than $E_{V,seg}$ (–0.54 eV).

Figure 4 (a) shows the change of the electrostatic poten-

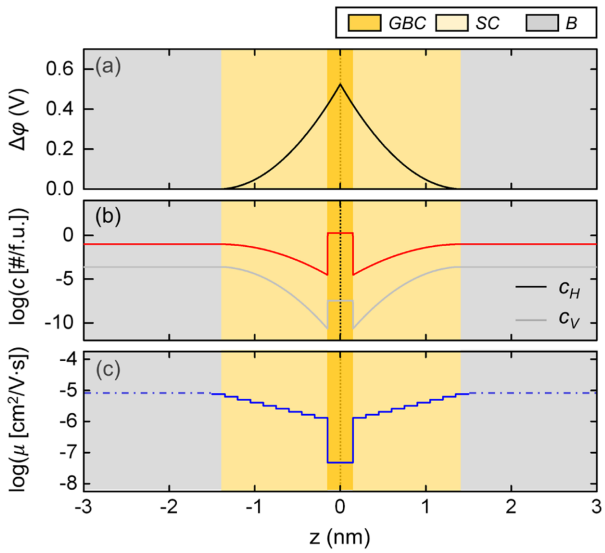

Fig. 4. (a) Δφ, (b) c_H and c_V, and (c) the proton mobility as a function of z at 600 K, where dark yellow, light yellow, and grey zones are *GBC*, *SCL*, and *B*, respectively.

tial, $\varphi(z)$, as a function of z at 600K. Dark yellow, light yellow, and grey zones indicate *GBC*, *SCL*, and *B*, respectively. As a consequence of the segregated H to the grain boundary region, a Schottky barrier height ($\Delta\varphi(0)$) as calculated by the following equation appeared in the grain boundary core.

$$\Delta\varphi(0) = \varphi(0) - \varphi(\infty)$$

Here, $\varphi(0)$ and $\varphi(\infty)$ are electrostatic potentials in the grain boundary core and far away from it, respectively. We obtained $\Delta\varphi(0)$ of 0.52 V and *SCL* thickness (λ) of 1.46 nm at 600K. We found that these are very close to the values of 0.51 V and 1.41 nm, respectively, reported by Yang *et al.*[13]

Figure 4 (b) shows change of c_H and c_V (represented by red and grey lines, respectively) as a function of z at 600K. c_H is high at the *GBC*, but c_V with the same positive charge is very low. In the *SCL* region right next to the *GBC* of 0.3 nm, concentrations of c_H and c_V become very low, and increase gradually toward the *B* region.

Figure 4 (c) shows change of H mobility (μ_H^i, i = *GBC*, *SC*, *B*) as a function of z at 600K. The blue line stands for μ_H^{GBC} and μ_H^{SC}, and the blue dash-dotted line stands for μ_H^B. Referring the 12.5% Y-doped case,[32] we used E_m^B of 0.45 eV, and assumed that E_m^{SC} and E_m^B are the same. We referred the details of E_m^B and D_0 to the work by Yang *et al.*[13] For E_m^{GBC}, we used 0.61 eV which is the value when a proton passes through the minimum energy path across the grain boundary structure. H mobility across the grain boundary core, μ_H^{GBC}, was about 10^{-7} cm^2/V·s at 600 K, which is lower than μ_H^B of 10^{-5} cm^2/V·s.

Figure 5 shows change of proton conductivity as σT against reciprocal temperature (1000/T) based on the calculated c_H and μ_H by using the *SCL* and *SD* models. The black, blue, and red lines represent σ_H^B, σ_H^{GB} of the stoichiometric $\sum 3$ BZO(111)[1$\bar{1}$0], and σ_H^{GB} of nonstoichiometric one, respectively.[13] The grey filled and open symbols indicate the experimentally measured σ_H^B and σ_H^{GB} from the literature, respectively.[6-8] Note that the calculated σ_H^B shows the same trend with those by experiments, and that increase in temperature changes the slope of conductivity. This change in slope can attribute to the reduced c_H in bulk grain due to dehydration with increasing temperature.[13] σ_H^{GB} for both stoichiometric and nonstoichiometric grain boundaries are lower than that for grain interior, and display the same trend with experimental σ_H^{GB}. We concluded that stoichiometry has only minor effects on σ_H^{GB}, although σ_H^{GB} of the nonstoichiometric grain boundary shows slightly lower value.

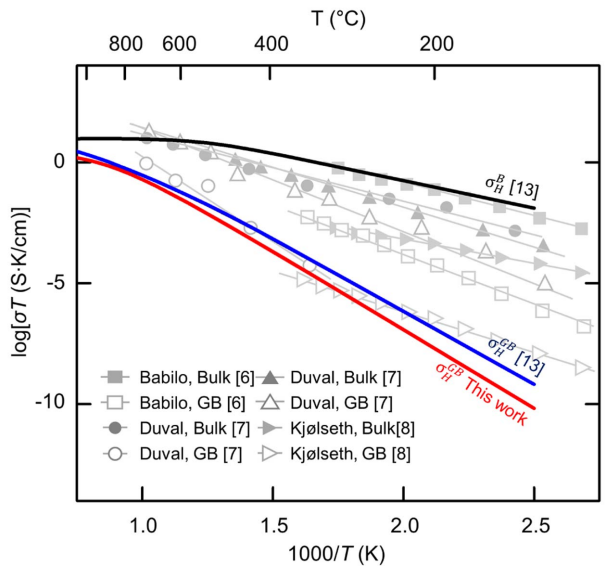

Fig. 5. σT as a function of inverse temperature (1000/T). The black, blue, and red lines indicate the σ_H^B, stoichiometric σ_H^{GB}, and nonstoichiometric σ_H^B, respectively. Grey filled and open symbols indicate the experimentally measured σ_H^B and σ_H^{GB} from literature, respectively.

4. Conclusions

We evaluate proton conduction for the nonstoichiometric $\sum 3$ $BaZrO_3$ (210)[001] tilt grain boundary using DFT. We introduce H and V into the grain boundary to calculate c_H and c_V using *SCL* model, and observe positional changes of energy. We confirm that both H and V prefer to segregate to the grain boundary core to be more stable with $E_{H,seg}$ and $E_{V,seg}$ of –0.70 and –0.54 eV, respectively. The barrier energy for H crossing the grain boundary core is 0.61 eV by the *SD* model, which leads to calculation of μ_H. We conclude that stoichiometry has only minor effects on σ_H^{GB}, although σ_H^{GB} of the nonstoichiometric grain boundary shows slightly lower value.

Acknowledgments

This study is supported by the Fusion Research Program for Green Technologies through the National Research Foundation (NRF) of Korea funded by the Ministry of Education, Science and Technology (2011-0019304), and by the KIST Institutional Program (Project No. 2E24021).

REFERENCES

1. T. Takahashi and H. Iwahara, "Proton Conduction in Perovskite Type Oxide Solid Solution," *Rev. Chim. Miner.*, **17** 243-53 (1980).
2. H. Iwahara, T. Esaka, H. Uchida, and N. Maeda, "Proton Conduction in Sintered Oxide and its Application to Steam Electrolysis for Hydrogen Production," *Solid State Ionics*, **3–4** 359-63 (1981).
3. K. D. Kreuer, "Proton-Conducting Oxides," *Annu. Rev. Mater. Res.*, **33** 333-59 (2003).
4. T. Norby and Y. Larring, "Concentration and Transport of Protons in Oxides," *Curr. Opin. Solid State Mater. Sci.*, **2** [5] 593-99 (1997).
5. F. Iguchi, N. Sata, T. Tsurui, and H. Yugami, "Microstructures and Grain Boundary Conductivity of $BaZr_{1-x}Y_xO_3$ (x = 0.05, 0.10, 0.15) Ceramics," *Solid State Ionics*, **178** [7] 691-

95 (2007).
6. P. Babilo, T. Uda, and S. M. Haile, "Processing of Yttrium-doped Barium Zirconate for High Proton Conductivity," *J. Mater. Res.*, **22** [5] 1322-30 (2007).
7. S. B. C. Duval, P. Holtappels, U. F. Vogt, E. Pomjakushina, K. Conder, U. Stimming, and T. Graule, "Electrical Conductivity of the Proton Conductor $BaZr_{0.9}Y_{0.1}O_{3-\delta}$ Obtained by High Temperature Annealing," *Solid State Ionics*, **178** [25] 1437-41 (2007).
8. C. Kjølseth, H. Fjeld, Ø. Prytz, P. I. Dahl, C. Estournès, R. Haugsrud, and T. Norby, "Space–Charge Theory Applied to the Grain Boundary Impedance of Proton Conducting $BaZr_{0.9}Y_{0.1}O_{3-\delta}$," *Solid State Ionics*, **181** [5] 268-75 (2010).
9. E. E. Helgee, A. Lindman, and G. Wahnström, "Origin of Space Charge in Grain Boundaries of Proton-Conducting $BaZrO_3$," *Fuel Cells*, **13** [1] 19-28 (2013).
10. J. M. Polfus, K. Toyoura, F. Oba, I. Tanaka, and R. Haugsrud, "Defect Chemistry of a $BaZrO_3$ Σ3 (111) Grain Boundary by First Principles Calculations and Space–Charge Theory," *Phys. Chem. Chem. Phys.*, **14** [35] 12339-46 (2012).
11. A. Lindman, E. E. Helgee, J. Nyman, and G.Wahnström, "Oxygen Vacancy Segregation in Grain Boundaries of $BaZrO_3$ Using Interatomic Potentials," *Solid State Ionics*, **230** 27-31 (2013).
12. B. J. Nyman, E. E. Helgee, and G. Wahnström, "Oxygen Vacancy Segregation and Space-Charge Effects in Grain Boundaries of Dry and Hydrated $BaZrO_3$," *Appl. Phys. Lett.*, **100** [6] 061903 (2012).
13. J.-H. Yang, D.-H. Kim, B.-K. Kim, and Y.-C. Kim, "Calculation of Proton Conductivity at the Σ3(111)/[1$\bar{1}$0] Tilt Grain Boundary of Barium Zirconate Using Density Functional Theory," *Solid State Ionics,* **279** 60-5 (2015).
14. M.-Y. Kim, G. Duscher, N. D. Browning, K. Sohlberg, S. T. Pantelides, and S. J. Pennycook, "Nonstoichiometry and the Electrical Activity of Grain Boundaries in $SrTiO_3$," *Phys. Rev. Lett.*, **86** [18] 184056-59 (2001).
15. S.-Y. Choi, S. Joong, L. Kang, S.-Y. Chung, T. Yamamoto, and Y. Ikuhara, "Change in Cation Nonstoichiometry at Interfaces during Crystal Growth in Polycrystalline $BaTiO_3$," *App. Phys. Lett.*, **88** [1] 011909-3 (2006).
16. J.-S. Kim, J.-H. Yang, B.-K. Kim, and Y.-C. Kim, "Study of Σ3 $BaZrO_3$ (210)[001] Tilt Grain Boundaries Using Density Functional Theory and a Space Charge Layer Model," *J. Ceram. Soc. Jpn.*, **123** [4] 245-49 (2015).
17. G. Kresse and J. Hafner, "*Ab initio* Molecular Dynamics for Liquid Metals," *Phys. Rev. B*, **47** 558-61 (1993).
18. G. Kresse, *Ab initio* Molekular Dynamik für flüssige Metalle, in Ph.D. Thesis, Technische Universität Wien, Wien, 1993.
19. G. Kresse and J. Furthmüller, "Efficiency of ab-initio Total Energy Calculations for Metals and Semiconductors Using a Plane-Wave Basis Set," *Comput. Mater. Sci.*, **6** [1] 15-50 (1996).
20. G. Kresse and J. Furthmüller, "Efficient Iterative Schemes for *ab initio* Total-Energy Calculations Using a Plane-Wave Basis Set," *Phys. Rev. B,* **54** [16] 11169-86 (1996).
21. G. Kresse and D. Joubert, "From Ultrasoft Pseudopotentials to the Projector Augmented-Wave Method," *Phys. Rev. B*, **59** [3] 1758-75 (1999).
22. P. E. Blöchl, "Projector Augmented-Wave Method," *Phys. Rev. B,* **50** [24] 17953-79 (1994).
23. J.P. Perdew, K. Burke, and M. Ernzerhof, "Generalized Gradient Approximation Made Simple," *Phys. Rev. Lett.*, **77** [18] 3865-68 (1996).
24. S. L. Dudarev, G. A. Botton, S. Y. Savrasov, C. J. Humphreys, and A. P. Sutton, "Electron-Energy-Loss Spectra and the Structural Stability of Nickel Oxide: An LSDA+U study," *Phys. Rev. B,* **57** [3] 1505-9 (1998).
25. V. Stevanovic, S. Lany, X. Zhang, and A. Zunger, "Correcting Density Functional Theory for Accurate Predictions of Compound Enthalpies of Formation: Fitted Elemental-Phase Reference Energies," *Phys. Rev. B*, **85** [11] 115104-12 (2012).
26. H. J. Monkhorst and J. D. Pack, "Special Points for Brillouin-Zone Integrations," *Phys. Rev. B*, **13** [12] 5188-92 (1976).
27. W. Tang, E. Sanville, and G. Henkelman, "A Grid-based Bader Analysis Algorithm without Lattice Bias," *J. Phys.: Condens. Matter,* **21** [8] 084204 (2009).
28. G. Henkelman, B. P. Uberuaga, and H. Jónsson, "A Climbing Image Nudged Elastic Band Method for Finding Saddle Points and Minimum Energy Paths," *J. Chem. Phys.,* **113** [22] 9901-4 (2000).
29. K. Momma and F. Izumi, "VESTA: A Three-Dimensional Visualization System for Electronic and Structural Analysis," *J. Appl. Cryst.*, **41** [3] 653-58 (2008).
30. S. Yamanaka, M. Fujikane, T. Hamaguchi, H. Muta, T. Oyama, T. Matsuda, S. Kobayashi, and K. Kurosaki, "Heat Capacities and Thermal Conductivities of Perovskite Type $BaZrO_3$ and $BaCeO_3$," *J. Alloys Compd.*, **359** [1] 1-4 (2003).
31. R. A. De Souza, "The Formation of Equilibrium Space-Charge Zones at Grain Boundaries in the Perovskite Oxide $SrTiO_3$," *Phys. Chem. Chem. Phys.,* **11** [43] 9939-69 (2009).
32. H. G. Bohn and T. Schober, "Electrical Conductivity of the High-Temperature Proton Conductor $BaZr_{0.9}Y_{0.1}O_{2.95}$," *J. Am. Ceram. Soc.*, **83** [4] 768-72 (2000).
33. M. A. Gomez, M. Chunduru, L. Chigweshe, L. Foster, S. J. Fensin, K. M. Fletcher and L. E. Fernandez, "The Effect of Yttrium Dopant on the Proton Conduction Pathways of $BaZrO_3$, a Cubic Perovskite," *J. Chem. Phys.,* **132** [21] 214709 (2010).